J. Fluid Mech. (1976), *vol.* 74, *part* 4, *pp.* 695–719
Printed in Great Britain

An experimental and theoretical study of natural convection in the annulus between horizontal concentric cylinders

By T. H. KUEHN AND R. J. GOLDSTEIN
Department of Mechanical Engineering, University of Minnesota, Minneapolis

(Received 6 October 1975)

An experimental and theoretical–numerical investigation has been carried out to extend existing knowledge of velocity and temperature distributions and local heat-transfer coefficients for natural convection within a horizontal annulus. A Mach–Zehnder interferometer was used to determine temperature distributions and local heat-transfer coefficients experimentally. Results were obtained using water and air at atmospheric pressure with a ratio of gap width to inner-cylinder diameter of 0·8. The Rayleigh number based on the gap width varied from $2{\cdot}11 \times 10^4$ to $9{\cdot}76 \times 10^5$. A finite-difference method was used to solve the governing constant-property equations numerically. The Rayleigh number was changed from 10^2 to 10^5 with the influence of Prandtl number and diameter ratio obtained near a Rayleigh number of 10^4. Comparisons between the present experimental and numerical results under similar conditions show good agreement.

1. Introduction

Natural convective heat transfer from a body to a finite space enclosing it has received increased attention in recent years. Applications have included nuclear reactor design, cooling of electronic equipment, aircraft cabin insulation and thermal storage systems. The horizontal concentric cylinder geometry is used in pressurized-gas underground electric transmission cables (Pedersen, Doepken & Bolin 1971).

Natural convection between horizontal concentric isothermal cylinders was first studied by Beckmann (1931), who used air, hydrogen and carbon dioxide to obtain overall heat-transfer coefficients. A similar investigation using air was made concurrently by Voigt & Krischer (1932). Kraussold (1934) extended these results to larger Prandtl numbers by using water, transformer oil and machine oil. He developed a correlation for the overall heat-transfer coefficients, including the data from Beckmann. Liu, Mueller & Landis (1961) measured the overall heat-transfer and radial temperature profiles of air, water and a silicone fluid. Qualitative flow descriptions were given for each fluid. Photographs of flow patterns in air using smoke were presented by Bishop & Carley (1966) and Bishop, Carley & Powe (1968). Different flow regimes depending on the Grashof number and diameter ratio were delineated by Powe, Carley & Bishop (1969).

The first determination of local heat-transfer coefficients in an annular geometry with air was made by Eckert & Soehngen (1948) using a Mach–Zehnder interferometer. Grigull & Hauf (1966) used a similar technique to measure the local heat-transfer coefficients in air on the inner cylinder for nine diameter ratios. Koshmarov & Ivanov (1973) obtained overall heat-transfer data for Grashof numbers between 10^{-9} and 10^{5}, including results in the rarefied-gas regime. Other Soviet studies include Zagromov & Lyalikov (1966) and Berkengeim (1966). The only investigation into the turbulent regime has been made by Lis (1966), who also obtained results using axial spacers. Nitrogen and sulphur hexafluoride mixtures were used at pressures from 0·7 to 40 atm, resulting in Rayleigh numbers up to 10^{10}. Overall heat-transfer measurements were made as well as schlieren photographs of the flow.

Several correlations have been proposed for experimental mean heat-transfer data for natural convection in horizontal annuli, with the results often given in terms of an equivalent conductivity. The equivalent conductivity is defined as the actual heat flux divided by the heat flux that would occur by pure conduction in the absence of fluid motion. Bishop (1966) found that the mean equivalent conductivity is essentially a function of the Rayleigh number based on the gap thickness for various diameter ratios. A better fit was obtained by Itoh *et al.* (1970), who used $(R_i R_o)^{\frac{1}{2}} \ln (R_i/R_o)$, where R_i and R_o are the inner and outer cylinder radii, as the characteristic length in the Rayleigh number. Raithby & Hollands (1975) used a conduction-layer model similar to that used by Langmuir as reported by Eckert (1960). A slightly different approach was used by Barelko & Shtessel (1973) that is more general.

Four analytical solutions valid at small Rayleigh numbers have been obtained. Mack & Bishop (1968) used a power-series expansion for natural convection between isothermal concentric cylinders. Hodnett (1973) used a perturbation method in dealing with the same problem. Huetz & Petit (1974) considered the case of constant heat flux on one wall, the other remaining isothermal. The conjugate problem of conduction within the inner cylinder coupled with convection in the gap has been studied by Rotem (1972).

The first numerical solution for natural convection between horizontal concentric cylinders was obtained by Crawford & Lemlich (1962) using a Gauss–Seidel iterative approach. Abbott (1964) used matrix inversion techniques to obtain solutions for very thin gaps. Shibayama & Mashimo (1968) compared their theoretical streamlines with photographs of smoke patterns in air. Powe, Carley & Carruth (1971) examined the transition to unsteady flow for Prandtl numbers near 0·7 by determining the Rayleigh number at which a counter-rotating eddy began to form. They found that this agreed with the previous experimental determinations of Powe *et al.* (1969).

Although qualitative comparisons between flow patterns obtained experimentally and theoretically have been made for the concentric cylinder configuration (Shibayama & Mashimo 1968), there has been very little direct quantitative comparison of heat-transfer results. In the present study, natural convection between horizontal concentric cylinders is investigated experimentally with optical methods and theoretically using numerical techniques. The range of

conditions used in each method overlaps so that the heat-transfer results can be compared quantitatively.

The experimental results are obtained with the aid of a Mach–Zehnder interferometer. This technique enables the temperature field in the enclosure to be visualized. Since the flow investigated is assumed steady with no axial variation except for end effects, the results can be interpreted as the temperature distribution at any cross-section. This also permits values for the local heat flux to be determined. Local heat-transfer coefficients are obtained on both cylinders with either air or water in the annulus.

Numerical solutions of the governing equations with the constant-property assumption provide both the temperature and the velocity distribution. From these, the local and overall heat-transfer coefficients are obtained and compared with the experimental results. The present solutions extend previous results to higher Rayleigh numbers and show the effect of Prandtl number and diameter ratio.

2. Experimental study

Apparatus

A test cell was built for use in a Mach–Zehnder interferometer capable of using air at atmospheric pressure as well as liquids. Interferograms record the temperature distribution between the cylinders, which can be analysed to yield the local heat flux. The assembled apparatus with the thin windows in place is shown in figure 1.

The inner cylinder was machined from solid copper bar stock into a tube 20·3 cm long with an outside diameter of 3·56 cm and a wall thickness of 0·51 cm. This was heated by passing direct current through a 100 Ω tubular resistor approximately 18 cm long held in the centre of the cylinder. Six thermocouples, four in the mid-plane spaced 90° apart and one at each end, were positioned within 2 mm of the outer surface of the cylinder. All thermocouple and heater wires were passed through a slot near one end. Expanded polystyrene disks were mounted on each end to reduce conduction losses to the windows. The inner cylinder was held concentrically within the outer cylinder by two stainless-steel hanger rods about 2 mm in diameter.

The outer cylinder, also of copper, was machined into a tube 20·32 cm long with an inside diameter of 9·25 cm and a wall thickness of 0·45 cm. This made $L/D_i = 0{\cdot}8$, where L is the annulus gap width and D_i is the outside diameter of the inner cylinder. Six thermocouples were positioned within 1 mm of the inside surface and located in a similar fashion to those in the inner cylinder. Two copper strips 1·27 cm wide and 0·1 cm thick were placed around the outside to form flow channels for the cooling water in the form of a double helix. This permitted counterflow of water in adjacent passages. The strips, which were soldered onto the outer cylinder, also act as fins to increase the heat-transfer coefficient to the cooling water. Brass flanges soldered onto each end of the outer cylinder hold the windows in place and serve as end supports for a larger brass cylinder that forms the enclosure for the cooling passages.

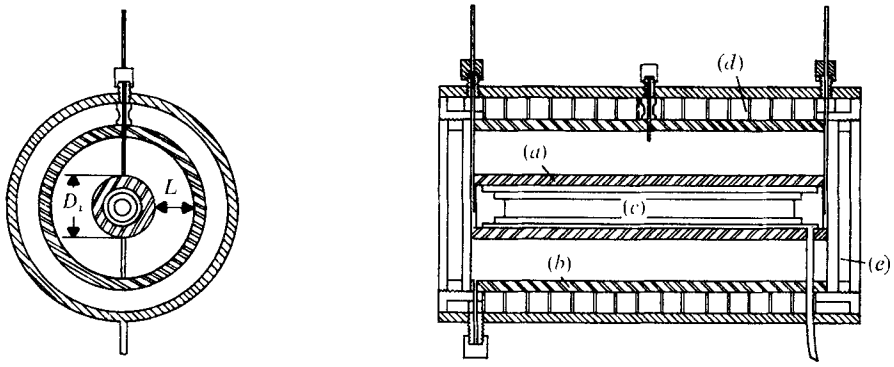

FIGURE 1. Schematic diagram of experimental apparatus. (*a*) Inner cylinder. (*b*) Outer cylinder. (*c*) Heater. (*d*) Cooling water channels. (*e*) Window.

Two sets of windows were used depending upon the fluid. Windows 10·13 cm in diameter and 0·585 cm thick were used with air. These were cut from selected pieces of commercially available polished plate glass. When water was used, these caused optical distortions from bending due to hydrostatic loading. Two windows 5·08 cm thick were made that prevented this and enabled good isothermal infinite-fringe settings to be obtained.

Electric power was provided to the inner-cylinder resistor by a regulated d.c. power supply. The power input was read from a wattmeter with an accuracy of $\pm$ 0·04 W. The cooling water was maintained isothermal to within $\pm$ 0·01 °C by a constant-temperature water bath. The thermocouples were connected separately for the air runs so that any non-uniformities in temperature on either cylinder could be measured. When water was used the thermocouples were placed in series to form two thermopiles, one for each cylinder. The individual thermocouples could be read to within 0·02 °C and the thermopiles to within 0·004 °C. The maximum angular temperature difference was found to be 0·2 % of the temperature difference between the cylinders for the inner cylinder and 0·1 % for the outer cylinder. The maximum axial variations were 1 and 0·03 % for the inner and outer cylinders respectively.

The principle of operation of the Mach–Zehnder interferometer is described by numerous authors including Goldstein (1970) and Hauf & Grigull (1970). The light source was a 5 mW helium–neon laser. No compensating chamber was required.

Procedure

Two sets of experimental runs were made, one with air, the other using water. For the air runs the thin windows were set in place after the two cylinders had been positioned concentrically. When water was used, the thick windows were mounted and the cell filled with demineralized water that had been boiled to reduce the amount of dissolved gasses. After this the entire test cell was insulated and left overnight to come to thermal equilibrium.

The cell was then aligned with the test beam of the interferometer, which had previously been adjusted to be horizontal. An isothermal infinite-fringe setting

was obtained by rotating the mirrors of the interferometer. Photographs, both with and without the reference beam, were taken to determine the scale factor and to record the uniformity of the optical adjustment. Then the cooling water was circulated and the power supply adjusted to a predetermined setting. The apparatus was left to reach a steady state, which took at least 3 h for the air runs and up to 8 h for the water runs.

The data acquisition consisted of reading the temperatures of the room and water bath, measuring the thermocouple e.m.f.'s, recording the local atmospheric pressure and determining the power input to the inner cylinder. After all of these had been satisfactorily recorded, a number of interferograms were made as well as a photograph with the reference beam blocked so that refraction effects could be observed. These were taken on 35 mm fine-grain film.

Mean heat-transfer results consisted of the average equivalent conductivity, Rayleigh number and Prandtl number obtained from the wattmeter, thermocouples and barometric pressure reading. All fluid properties were evaluated at the arithmetic mean of the temperatures of the two cylinders. End-loss and radiation corrections were needed for the air results; only a minor end-loss correction was necessary when using water. The end loss due to conduction through the windows was found by filling the annulus with an insulating material of known thermal conductivity and measuring the total amount of heat transported between the cylinders at various temperature differences. The corrected total heat flow agreed with the averaged fringe values, so that heat transfer between the fluid and the windows was neglected.

Local results were obtained from the interferograms. The position of each fringe was measured by viewing the film negative on a tool-maker's microscope. Readings were necessary on only half of the interferogram owing to symmetry. The positions were measured along radial lines starting near the inner-cylinder surface. This procedure was followed at least every 30° with 15° intervals used when more complete data were desired. Corrections for first- and second-order refraction errors as well as thick-window effects were included in the data reduction. The only external input required was the temperature of one of the *cylinders from the thermocouple measurements and the atmospheric pressure* when air was used. The temperature corresponding to each fringe was obtained by starting at the cylinder with the known temperature and index of refraction and proceeding towards the other. The three points closest to each cylinder were fitted with a straight line using a least-squares regression analysis. This provided the temperature gradient and the local heat flux at each surface. The temperature difference and Rayleigh number were found at every angle by extrapolating these lines to the position of each surface. The averaged fringe heat-transfer results were obtained by averaging the local equivalent conductivities and temperature differences for the various angles.

The mean heat-transfer results were used as a check on the Rayleigh number and the total heat flux as determined from the interferograms. The two methods agreed to within 7 % for the Rayleigh number and to within 3 % for the total heat flux. The mean results were also used where interferometer data could not be obtained owing to large refraction effects.

Results

Since most of the data were obtained from the interferograms, the majority of the discussion below is based on optical measurements. An interferogram using air is shown in figure 2 (plate 1). The fringes can be considered to represent isotherms since the index of refraction is a function of temperature only.

The inner-cylinder boundary layer resembles the natural convection boundary layer near a single horizontal cylinder. The radial fringe spacing near the cylinder surface is smallest at the bottom. This indicates that the largest temperature gradient and heat flux occur on the bottom. The boundary-layer thickness increases as the flow moves up around the cylinder. The largest thickness and smallest temperature gradient occur at the separation point on top. The buoyant plume above the inner cylinder impinges upon the outer cylinder at the top, creating the thinnest boundary layer and highest heat flux for the system. This warm fluid then moves in a boundary layer adjacent to the outer cylinder towards the bottom. In part of the region between the two boundary layers a temperature inversion exists, the fluid near the cool surface being warmer than that closer to the heated surface. This phenomenon has also been observed in natural convection in a vertical slot (MacGregor & Emery 1968) and between concentric spheres (Scanlan, Bishop & Powe 1970).

The flow has been found to be unsteady at high Rayleigh numbers ($> 10^5$) by other investigators. No oscillations were observed in any of the present tests, which were at $Ra_L < 10^5$ with air. This is in good agreement with Powe *et al.* (1969).

An interferogram obtained using water is given in figure 3 (plate 2). The temperature distribution resembles that for air at the same Rayleigh number, including thermal boundary layers and the reversed temperature gradient near the centre of the gap. The isotherms comprising the inner-cylinder boundary layer tend to close at the top, creating a narrower thermal plume than in air. The temperature of the plume centre-line also decreases faster than for air. As expected from similarities in temperature distribution, the local heat-flux distribution is similar for air and water at the same Rayleigh number.

At higher Rayleigh numbers the temperature field alters, as can be observed in figure 4 (plate 3), taken using water at a Rayleigh number of $2{\cdot}33 \times 10^5$. The inner cylinder appears to be completely surrounded by a thermal boundary layer with large radial temperature gradients. The outer-cylinder boundary layer is well defined except near the bottom. The central core region has small horizontal temperature gradients in the centre near the 90° position. This region becomes larger as the Rayleigh number is increased. There is a small temperature dip adjacent to the edge of the inner-cylinder boundary layer and a warm hump next to the outer boundary layer. This was also found with thermocouple probes in water and higher Prandtl number fluids for natural convection between horizontal cylinders by Liu *et al.* (1961), between spheres by Scanlan *et al.* (1970) and in a vertical slot by MacGregor & Emery (1968). Rubel & Landis (1969) predicted this numerically for natural convection in a vertical slot for Rayleigh numbers based on the plate separation larger than 10^5. The present Rayleigh number is essentially equivalent since it is based on the distance between the cylinders.

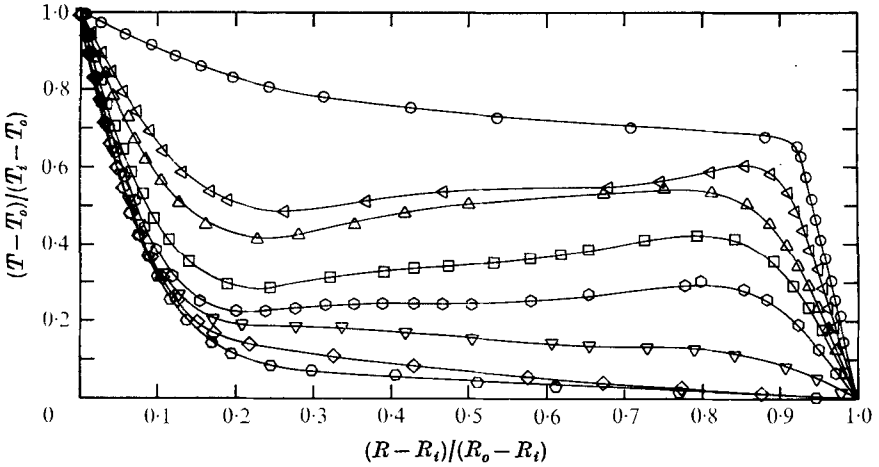

FIGURE 5. Dimensionless radial temperature distribution in water for $Ra_L = 2{\cdot}09 \times 10^5$, $Pr = 5{\cdot}45$, $L/D_i = 0{\cdot}8$. ○, 0°; ◁, 15°; △, 30°; □, 60°; ◊, 90°; ▽, 120°; ◇, 150°; ○, 180°.

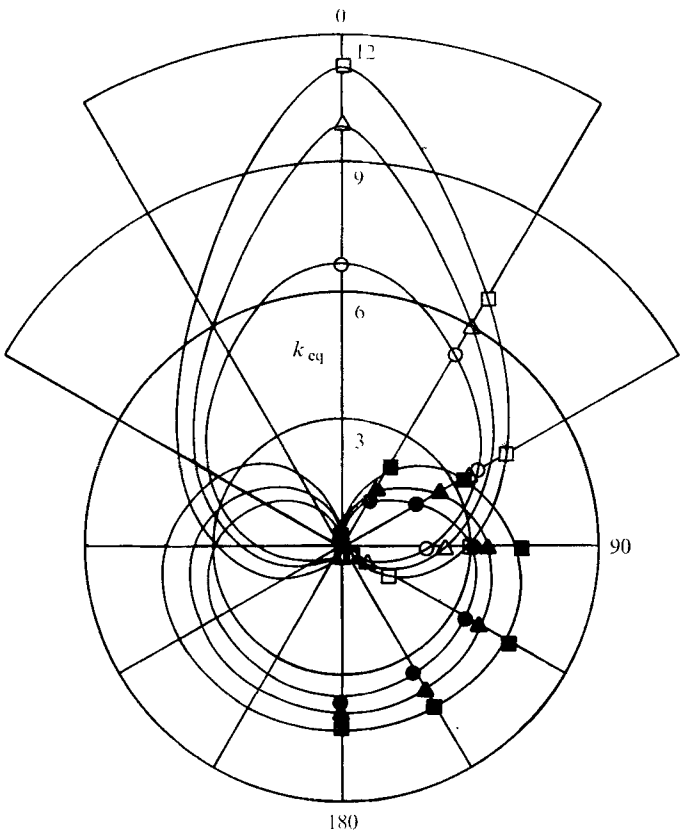

FIGURE 6. Influence of Rayleigh number on local equivalent conductivity in air.

Ra_L	Inner cylinder	Outer cylinder
$2{\cdot}66 \times 10^4$	●	○
$3{\cdot}65 \times 10^4$	▲	△
$8{\cdot}86 \times 10^4$	■	□

ΔT (°C)	$\frac{1}{2}(T_i+T_o)$ (°C)	Q (W)	Ra_L	Pr	$\bar{k}_{eq}$
		Results using air			
11·14	33·46	1·08	$2{\cdot}11\times10^4$	0·706	2·34
14·37	35·03	1·33	2·66	0·706	2·58
17·12	36·55	1·64	3·09	0·706	2·66
20·02	36·11	1·98	3·65	0·706	2·75
20·41	28·57	2·01	4·16	0·707	2·80
26·30	35·23	2·90	4·70	0·706	3·00
31·42	36·12	3·48	5·72	0·706	3·09
41·65	41·28	4·90	7·02	0·705	3·23
50·53	50·66	6·36	7·43	0·702	3·37
60·16	50·57	7·76	8·86	0·702	3·46
69·27	55·13	9·50	9·56	0·702	3·62
		Results using water			
0·039	31·00	0·102	$2{\cdot}32\times10^4$	5·33	2·55
0·075	27·72	0·188	3·76	5·76	2·86
0·109	27·31	0·298	5·32	5·82	3·10
0·163	28·43	0·489	8·46	5·67	3·42
0·224	24·72	0·670	9·52	6·21	3·70
0·191	30·86	0·519	$1{\cdot}12\times10^5$	5·34	3·78
0·242	31·24	0·821	1·46	5·30	4·03
0·318	29·64	1·02	1·76	5·50	-3·98
0·371	30·03	1·29	2·09	5·45	4·29
0·544	24·90	1·97	2·33	6·19	4·48
0·450	30·07	1·60	2·54	5·45	4·35
0·622	29·50	2·55	3·42	5·52	5·00
0·781	29·61	3·33	4·31	5·51	5·21
1·297	29·93	6·29	7·28	5·46	5·90
2·356	23·94	11·53	9·53	6·34	6·08
1·721	30·14	8·73	9·76	5·44	6·18

TABLE 1. Experimental mean heat-transfer results for $L/D_i = 0{\cdot}8$

The dimensionless radial temperature profiles for water are essentially similar to those for air below $Ra_L = 10^5$. Figure 5 shows the temperature profiles for one of the water tests above $Ra_L = 10^5$. The top vertical position is 0° with 180° at the bottom. The distribution is very similar to that measured in silicone fluid with a thermocouple by Liu *et al.* (1961) although the present Rayleigh number is smaller by a factor of 2. The thermal boundary layers near both cylinders are well defined, as is the temperature inversion in the central region.

The distributions of the local equivalent conductivities on both cylinders are shown in figure 6 for three different air runs. The distribution on the inner cylinder resembles that given by Grigull & Hauf (1966) for large L/D_i ratios. The largest value occurs at the stagnation point on the bottom with the minimum on the top. This is qualitatively similar to natural convection about a single horizontal cylinder. The highest heat transfer on the outer cylinder is on the top owing to the impinging plume. The values decrease from there until the bottom is reached,

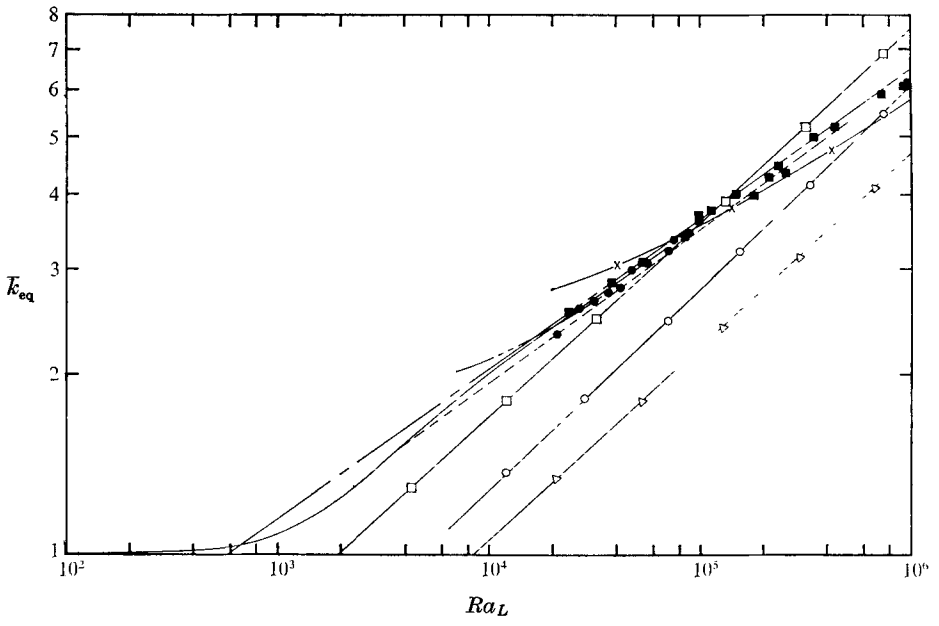

FIGURE 7. Mean equivalent conductivity as a function of Rayleigh number for the present experimental results, the present numerical results for $Pr = 0{\cdot}7$ and $L/D_i = 0{\cdot}8$ and previous correlations for $Pr \approx 0{\cdot}7$ and $L/D_i = 0{\cdot}8$. ●, present experiments using air; ■, present experiments using water; ——, present numerical results; —○—, Kraussold; —△—, Liu *et al.*; —×—, Lis; – – –, Bishop; — – – —, Shibayama & Mashimo; —◇—, Barelko & Shtessel; — – —, Raithby & Hollands.

which has practically zero heat flux. The distribution on the inner cylinder is the more uniform of the two.

The average equivalent conductivities for both the air and the water results are given in table 1. The values for water are slightly higher than those for air. The air data are correlated using a least-squares regression analysis by

$$\bar{k}_{eq} = 0{\cdot}159 Ra_L^{0{\cdot}272}, \quad 2{\cdot}1 \times 10^4 < Ra_L < 9{\cdot}6 \times 10^4, \tag{2.1}$$

and the water results by

$$\bar{k}_{eq} = 0{\cdot}234\, Ra_L^{0{\cdot}238}, \quad 2{\cdot}3 \times 10^4 < Ra_L < 9{\cdot}8 \times 10^5. \tag{2.2}$$

If one forced the data to fit a one-fourth power law, the correlations would be

$$\bar{k}_{eq} = 0{\cdot}200 Ra_L^{0{\cdot}25}, \quad \bar{k}_{eq} = 0{\cdot}202 Ra_L^{0{\cdot}25} \tag{2.3), (2.4}$$

for air and water respectively.

The present experimental results are shown in figure 7, as well as the present numerical curve for $L/D_i = 0{\cdot}8$ and $Pr = 0{\cdot}7$. Several previously obtained correlations are shown for comparison. The present results agree well with the experimental correlation of Bishop (1966) and the conduction-boundary-layer model *developed by Raithby & Hollands (1975) for* $L/D_i = 0{\cdot}8$. *The experimental* correlation given by Itoh *et al.* (1970) is not shown since the curve is nearly identical to that of Raithby & Hollands. The others do not agree as well with the

present results. The curves from Kraussold (1934) and Liu *et al.* (1961) are too low. Those of Shibayama & Mashimo (1968), Lis (1966) and Barelko & Shtessel (1973) with a critical Rayleigh number of 2×10^3 and $k = 0{\cdot}4$ are better but the slopes of these curves do not correspond to that of the present results.

3. Numerical study

Derivation of equations

To approximate the natural convection flow being studied, several assumptions have been made. Steady laminar flow is assumed since this has been found experimentally for small Rayleigh numbers. The flow is also assumed to be invariant along the axis of the cylinders, which leads to a two-dimensional approach. A vertical plane through the centre of the system divides the flow into two symmetric halves, so that only one side need be studied. The Boussinesq approximation of constant fluid properties is used. The governing equations commensurate with the above assumptions result in the following elliptic, coupled, time-independent equations in cylinderical polar co-ordinates:

$$\frac{\partial U}{\partial R}+\frac{U}{R}+\frac{1}{R}\frac{\partial V}{\partial \theta}=0, \tag{3.1}$$

$$\rho\left[U\frac{\partial U}{\partial R}+\frac{V}{R}\frac{\partial U}{\partial \theta}-\frac{V^2}{R}\right]=-\frac{\partial P}{\partial R}+\mu\left[\frac{\partial^2 U}{\partial R^2}+\frac{1}{R}\frac{\partial U}{\partial R}+\frac{1}{R^2}\frac{\partial^2 U}{\partial \theta^2}-\frac{U}{R^2}-\frac{2}{R^2}\frac{\partial V}{\partial \theta}\right]+F_R, \tag{3.2}$$

$$\rho\left[U\frac{\partial V}{\partial R}+\frac{V}{R}\frac{\partial V}{\partial \theta}+\frac{UV}{R}\right]=-\frac{1}{R}\frac{\partial P}{\partial \theta}+\mu\left[\frac{\partial^2 V}{\partial R^2}+\frac{1}{R}\frac{\partial V}{\partial R}+\frac{1}{R^2}\frac{\partial^2 V}{\partial \theta^2}-\frac{V}{R^2}+\frac{2}{R^2}\frac{\partial U}{\partial \theta}\right]+F_\theta, \tag{3.3}$$

$$\rho c\left[U\frac{\partial T}{\partial R}+\frac{V}{R}\frac{\partial T}{\partial \theta}\right]=k\left[\frac{\partial^2 T}{\partial R^2}+\frac{1}{R}\frac{\partial T}{\partial R}+\frac{1}{R^2}\frac{\partial^2 T}{\partial \theta^2}\right]. \tag{3.4}$$

The co-ordinates are R, measured from the centre of the system, and θ, measured clockwise from the upward vertical line. The radial velocity U is positive radially outwards, the angular velocity V positive in the clockwise direction for $0 \leqslant \theta \leqslant \pi$. P is the pressure, T the temperature and F_R and F_θ the body-force components in the radial and angular directions respectively. The fluid properties include the density ρ, dynamic viscosity μ, specific heat c and thermal conductivity k. The body-force terms can be written as functions of the temperature difference:

$$F_R = g\rho\beta(T-T_o)\cos\theta, \tag{3.5}$$

$$F_\theta = g\rho\beta(T-T_o)\sin\theta, \tag{3.6}$$

where g is the gravitational acceleration, T the temperature at a point within the fluid, T_o the temperature of the outer cylinder and β the thermal volumetric expansion coefficient. The stream function Ψ can be made to satisfy the continuity equation by setting $\quad U = R^{-1}\partial\Psi/\partial\theta, \quad V = -\partial\Psi/\partial R. \tag{3.7}$

After replacing the velocities with stream-function derivatives from (3.7) and F_R and F_θ by (3.5) and (3.6) the equations are made dimensionless by setting

$$\psi=\frac{\Psi}{\alpha}, \quad r=\frac{R}{L}, \quad \phi=\frac{T-T_o}{T_i-T_o}, \quad u=\frac{UL}{\alpha}, \quad v=\frac{VL}{\alpha}, \tag{3.8}$$

where $\alpha = k/\rho c$ is the thermal diffusivity, L is the gap between the cylinders and T_i is the temperature of the inner cylinder. The resulting equations can be simplified by introducing the vorticity, defined as

$$\omega = -\nabla^2\psi, \tag{3.9}$$

where

$$\nabla^2 = \frac{\partial^2}{\partial r^2}+\frac{1}{r}\frac{\partial}{\partial r}+\frac{1}{r^2}\frac{\partial^2}{\partial\theta^2}. \tag{3.10}$$

In the actual computations, it is convenient to use the velocities rather than the derivatives of the stream function in the coefficients. Therefore the equations to be solved are

$$\nabla^2\psi = -\omega, \tag{3.11}$$

$$\nabla^2\omega = \frac{1}{Pr}\left[u\frac{\partial\omega}{\partial r}+\frac{v}{r}\frac{\partial\omega}{\partial\theta}\right]+Ra_L\left[\sin\theta\frac{\partial\phi}{\partial r}+\frac{1}{r}\cos\theta\frac{\partial\phi}{\partial\theta}\right], \tag{3.12}$$

$$\nabla^2\phi = u\frac{\partial\phi}{\partial r}+\frac{v}{r}\frac{\partial\phi}{\partial\theta}, \tag{3.13}$$

along with the velocity equations (3.7). The dimensionless parameters appearing in the equations are the Prandtl number $Pr = \mu c/k$ and the Rayleigh number $Ra_L = \rho g\beta L^3(T_i - T_o)/\mu\alpha$. The values of the temperature and velocity at any position are determined by the Prandtl number, Rayleigh number, boundary conditions and geometry. For the concentric cylinder configuration the only geometry variable is the diameter ratio.

The boundary conditions imposed in the present problem are two impermeable isothermal walls at constant radii and two vertical lines of symmetry at $\theta = 0$ and $\theta = 180°$. The stream function is constant along each wall as well as along the lines of symmetry. Since no flow enters or escapes from the enclosure, the stream function is set equal to zero on all the boundaries. The dimensionless temperature equals unity on the inner cylinder and zero on the outer cylinder. It is assumed that at the lines of symmetry the angular derivatives of the temperature vanish. The vorticity is an odd function across the symmetry lines and equals zero on the symmetry lines. The value of the voriticity at the walls has been treated by numerous investigators, including Gosman *et al.* (1969, p. 116), who found the formulation of the vorticity at the walls to have a considerable effect on the convergence rate and stability of the computations. In the present case (3.11) is directly applied at the walls; the angular derivatives vanish, as does the first radial derivative of the stream function owing to the zero-velocity condition, leaving

$$\omega = -\partial^2\psi/\partial r^2. \tag{3.14}$$

Therefore the boundary conditions become

$$\psi = \partial u/\partial\theta = v = \omega = \partial\phi/\partial\theta = 0 \tag{3.15}$$

on the symmetry lines,

$$\psi = u = v = 0, \quad \omega = -\partial^2\psi/\partial r^2, \quad \phi = 1 \tag{3.16}$$

on the inner cylinder and

$$\psi = u = v = 0, \quad \omega = -\partial^2\psi/\partial r^2, \quad \phi = 0 \tag{3.17}$$

on the outer cylinder.

Method of solution

The finite-difference approach is used in the present problem to write the differential equations in terms of values at discrete points. The central-difference scheme that has truncation errors of second order in Δr and $\Delta\theta$ was found to be stable. This is used for the interior nodes while a one-sided difference formulation is required at the boundaries. For example, the temperature at an interior node (i, j) is given in terms of temperatures at surrounding nodes by

$$\phi_{i,j} = W_i \phi_{i+1,j} + X_i \phi_{i-1,j} + Y_i \phi_{i,j+1} + Z_i \phi_{i,j-1}, \tag{3.18}$$

where
$$W_i = \left(1 + \frac{\Delta r_i}{2r_i} - u_{i,j}\frac{\Delta r_i}{2}\right)\Big/ Q_i, \quad X_i = \left(1 - \frac{\Delta r_i}{2r_i} + u_{i,j}\frac{\Delta r_i}{2}\right)\Big/ Q_i, \tag{3.19a,b}$$

$$Y_i = \left(\frac{\epsilon_i^2}{r_i^2} - v_{i,j}\frac{\epsilon_i \Delta r_i}{2r_i}\right)\Big/ Q_i, \quad Z_i = \left(\frac{\epsilon_i^2}{r_i^2} + v_{i,j}\frac{\epsilon_i \Delta r_i}{2r_i}\right)\Big/ Q_i, \tag{3.19c,d}$$

with
$$Q_i = 2(1 + \epsilon_i^2/r_i^2), \quad \epsilon_i = \Delta r_i/\Delta\theta. \tag{3.19e}$$

i and j are integers describing the number of radial grid lines from the inner cylinder and the number of angular grid lines from the top symmetry line respectively. Similar relations were developed for the vorticity and stream function from (3.11) and (3.12).

The successive over-relaxation technique was chosen as the method of solution. This is a relatively simple method that can easily be altered when changing the grid structure or parameters affecting convergence. The major disadvantage is the task of choosing the optimum relaxation coefficients for a given situation. The temperature at an interior node is obtained from the following equation:

$$\phi_{i,j}^m = \phi_{i,j}^{m-1} + A(W_i \phi_{i+1,j}^n + X_i \phi_{i-1,j}^n + Y_i \phi_{i,j+1}^n + Z_i \phi_{i,j-1}^n - \phi_{i,j}^{m-1}), \tag{3.20}$$

where m is an integer equal to the number of the current iteration. The values at the surrounding nodes are the most recent at those points, so that n is either m or $m-1$ depending on the direction of the iteration-point sequence. The relaxation factor A used for ψ, ω and ϕ varied from 1·35, 0·5 and 1·2 respectively for Rayleigh numbers near 10^3 to 0·5, 0·05 and 0·5 near Rayleigh numbers of 10^5.

To keep the convergence time to a minimum without sacrificing accuracy, a semi-uniform grid was used with $\Delta r = 0{\cdot}05$ near the walls and 0·1 near the centre. The angular grid spacing was 10° except at large Rayleigh numbers, when the first angular grid space near the top was subdivided into four equal 2·5° increments. The basic grid was 16×19, giving a total of 304 nodes, 238 in the interior and 66 on the entire boundary.

The stream function and vorticity usually took longer to converge than the temperature. This was in part due to the smaller relaxation factor for the vorticity. In practice one complete iteration consisted of the sequence $\{\psi, \omega, \psi, \omega, \phi\}$, in which the first parameter was updated at every point, followed by the others in a similar manner.

The solution was considered to have converged when the stream function and temperature met the following criterion:

$$(B^m - B^{m-1})/B^{m-1} \leqslant c \tag{3.21}$$

at each point. Here B is either ψ or ϕ and c is a prespecified constant. For most solutions c was set equal to 10^{-3} but for some results above a Rayleigh number of 10^4 the value 5×10^{-3} was used. The vorticity usually did not satisfy this criterion since there was always one value very close to zero, causing the fraction to become very large. Another useful method for checking the convergence was to compare the average equivalent conductivities for the inner and outer cylinder. These were usually within 1 % at convergence.

The calculations were performed on a CDC 6600 digital computer using a Fortran program. The time required varied from about 10 s at Rayleigh numbers near 10^2 to about 90 s for Rayleigh numbers near 10^5, with running times averaging about 30*s*.

Results

Initially solutions were obtained that could be directly compared with previously published results. A solution similar to one presented by Crawford & Lemlich (1962) at $Ra_L = 8{\cdot}925 \times 10^3$, $Pr = 0{\cdot}714$ and $L/D_i = 0{\cdot}5$ was obtained. The results agree well, including the overall equivalent conductivity of 1·792 compared with the value 1·765 obtained previously.

An analytical result with $Ra_L = 1{\cdot}842 \times 10^3$, $Pr = 0{\cdot}7$ and $L/D_i = 0{\cdot}425$ presented by Mack & Bishop (1968) was also checked. The angular velocity and temperature distributions of the two studies agree fairly well although the results are not identical. The local equivalent conductivities differ by as much as 10 % although the mean value of 1·126 determined numerically is only about 2 % lower than that of 1·15 obtained before. The difference may be due to the slow convergence of the power series used by Mack & Bishop.

Another calculation was made under the conditions of a numerical solution obtained by Powe *et al.* (1971) with $Ra_L = 2{\cdot}767 \times 10^3$, $Pr = 0{\cdot}7$ and $L/D_i = 0{\cdot}1$. The flow results agree with the previous solution although the deviation of the local Nusselt number reported near the symmetry lines is not confirmed in the the present calculation. Perhaps the finite-difference formulation of the boundary conditions on the symmetry lines was not the same in both cases. A solution was also obtained at $Ra_L = 6 \times 10^3$, $Pr = 0{\cdot}7$ and $L/D_i = 0{\cdot}1$, which is above the transition line of Powe *et al.* (1969). A small counter-rotating eddy was found near the top of the annulus, extending about 15° from the top symmetry line. This is in good agreement with experimental observations of Powe *et al.* (1969).

Since one of the objectives of the current investigation is to compare the numerical results with the experiments, many solutions were obtained with $Pr = 0{\cdot}7$ and $L/D_i = 0{\cdot}8$. The Rayleigh number was increased from 10^2 to about 10^5. Over this range the flow is steady. This enabled the influence of the Rayleigh number on the flow and heat transfer to be studied. The following description of Rayleigh number effects pertains to $L/D_i = 0{\cdot}8$ although qualitatively similar results will exist for other diameter ratios.

The flow and heat-transfer results can be divided into several regimes. Below a Rayleigh number of 10^2 the maximum stream function or centre of rotation is near 90°. The flow in the top and bottom portions of the annulus is symmetric about the 90° position. The velocity profiles at any one position are similar, with

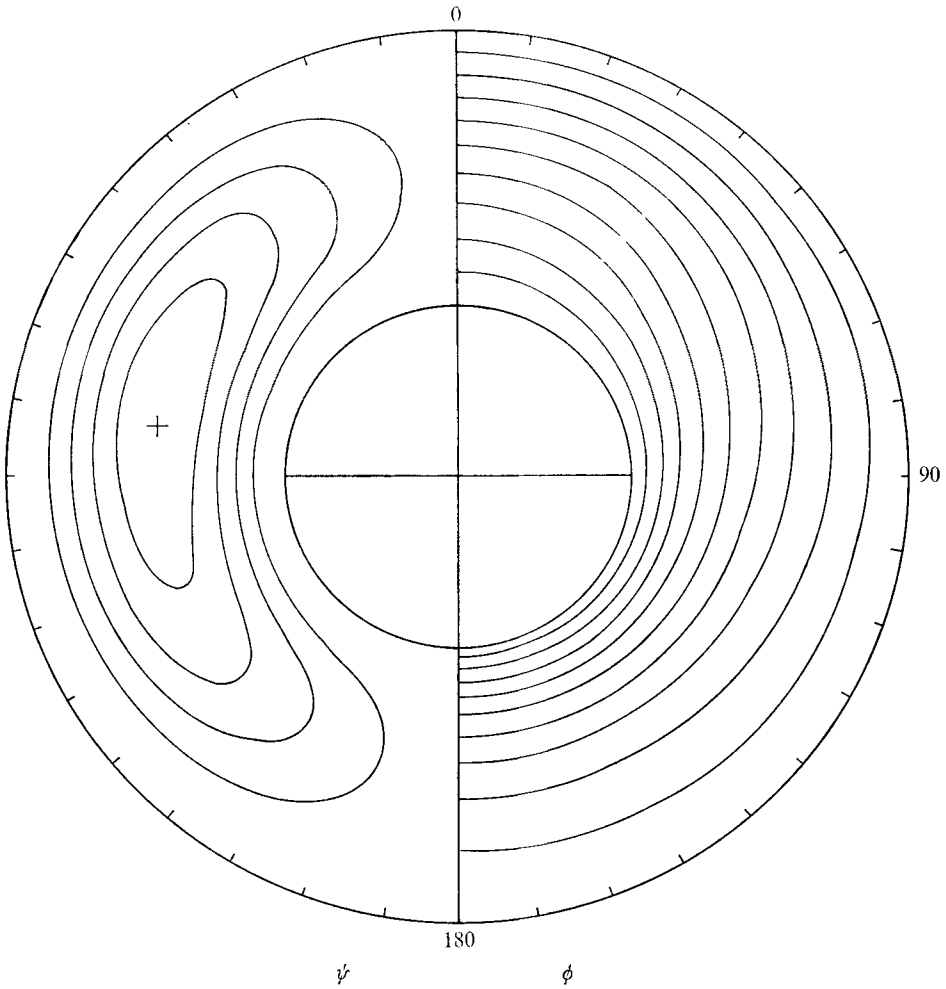

FIGURE 8. Streamlines and isotherms in transition region for $Ra_L = 10^3$, $Pr = 0{\cdot}7$, $L/D_i = 0{\cdot}8$, $\Delta\psi = 0{\cdot}5$, $\Delta\phi = 0{\cdot}1$.

the magnitudes directly proportional to the Rayleigh number. The velocities are too small to affect the temperature distribution, which remains essentially as in pure conduction. This makes the convection terms in (3.12) and (3.13) vanish. Therefore (3.12) and (3.13) can be approximated by

$$\nabla^2\omega = Ra_L\left[\sin\theta\frac{\partial\phi}{\partial r}+\frac{1}{r}\cos\theta\frac{\partial\phi}{\partial\theta}\right] \tag{3.22}$$

and

$$\nabla^2\phi = 0, \tag{3.23}$$

where the source term in (3.22) remains a constant times the Rayleigh number at any one position.

A transition region exists for Rayleigh numbers between 10^2 and 3×10^4. The flow remains in essentially the same pattern but becomes strong enough to

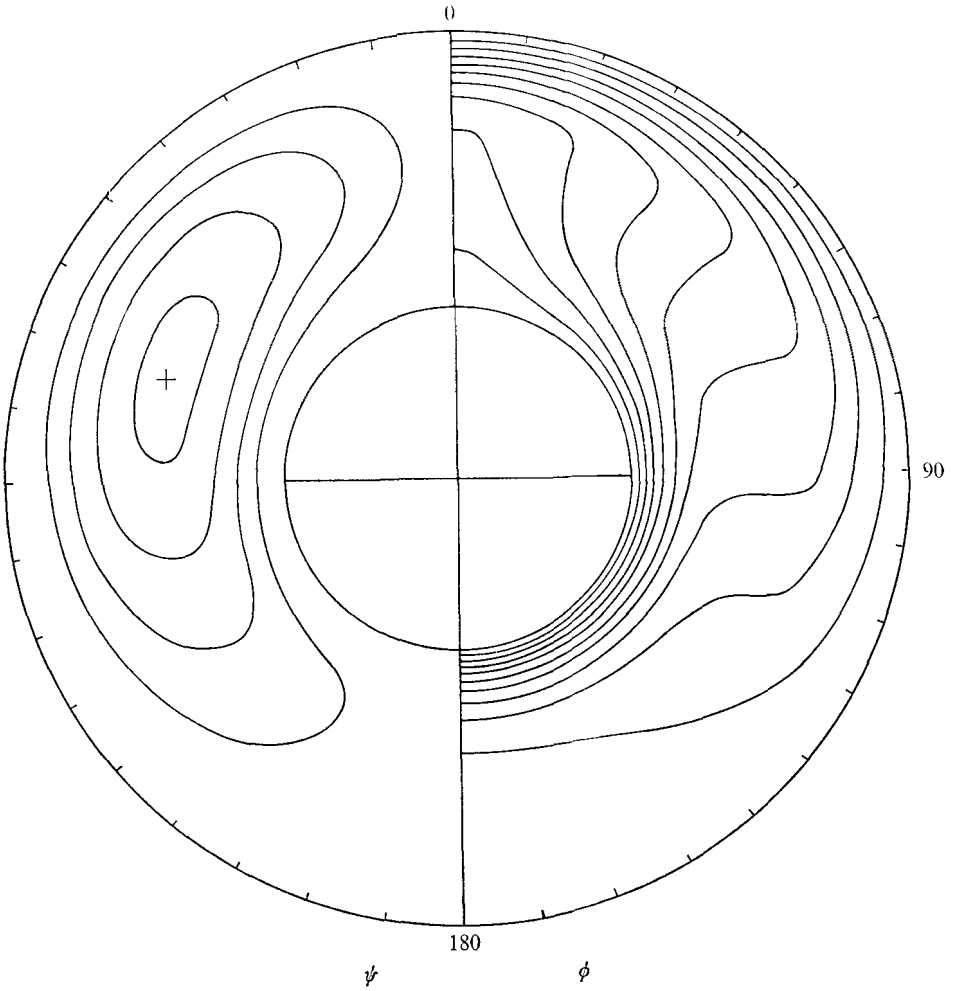

FIGURE 9. Streamlines and isotherms in transition region for $Ra_L = 10^4$, $Pr = 0{\cdot}7$, $L/D_i = 0{\cdot}8$, $\Delta\psi = 3{\cdot}0$, $\Delta\phi = 0{\cdot}1$.

influence the temperature field. As the Rayleigh number increases, the centre of rotation moves upwards.

The isotherms begin to resemble eccentric circles near a Rayleigh number of 10^3, as can be seen in figure 8. This has been called the 'pseudo-conductive regime' by Grigull & Hauf (1966) since the overall heat transfer remains essentially that of conduction. With further increases in Rayleigh number the temperature distribution becomes distorted, resulting in an increase in overall heat transfer.

A plot of streamlines and isotherms at a Rayleigh number of 10^4 is given in figure 9. Near this Rayleigh number, the radial temperature inversion appears, indicating the separation of the inner- and outer-cylinder thermal boundary layers. The cross indicates the location of the maximum value of the stream function, which would be the centre of rotation. This maximum is located near the 70° position with the flow above and below this being fairly symmetric. Local

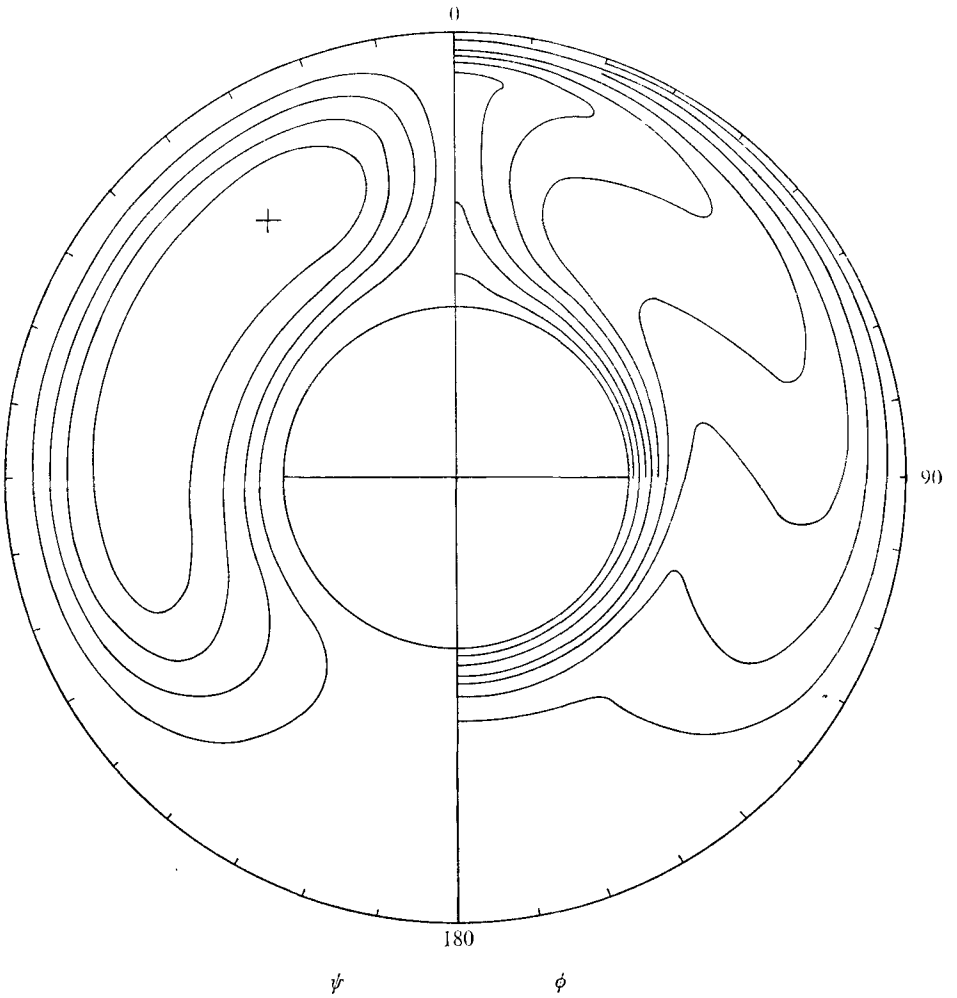

FIGURE 10. Streamlines and isotherms in steady laminar boundary-layer region for $Ra_L = 5 \times 10^4$, $Pr = 0{\cdot}7$, $L/D_i = 0{\cdot}8$, $\Delta\psi = 5{\cdot}0$, $\Delta\phi = 0{\cdot}1$.

heat-flux values are becoming further distorted from those of conduction. Essentially heat is being convected from the lower portion of the inner cylinder to the top of the outer cylinder. The vorticity in the central core is almost constant, indicating a region approaching solid-body rotation. This result was predicted for flow in a vertical slot by Batchelor (1954).

A steady laminar boundary-layer regime exists between Rayleigh numbers of 3×10^4 and 10^5. Streamlines and isotherms in this region are shown in figure 10. Boundary layers exist on both cylinders although the lower portion of the annulus is practically stagnant. The dimensionless radial temperature profiles in the inner-cylinder boundary layer are similar at a given angle when a distance scaling factor of $Ra_L^{\frac{1}{4}}$ is used. This is the same scaling factor as for a natural convection boundary layer about a single horizontal cylinder. Figure 11 shows the angular velocity distribution for $Ra_L = 5 \times 10^4$, $Pr = 0{\cdot}7$ and $L/D_i = 0{\cdot}8$. The Rayleigh

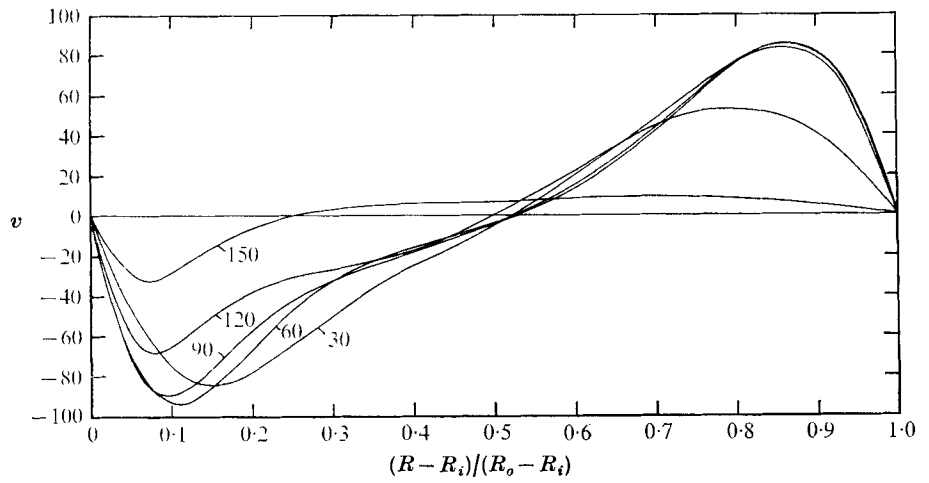

FIGURE 11. Angular velocity distribution in steady laminar boundary-layer region for $Ra_L = 5 \times 10^4$, $Pr = 0{\cdot}7$, $L/D_i = 0{\cdot}8$.

number based on the inner-cylinder diameter is $2{\cdot}56 \times 10^4$. The velocities near the inner cylinder resemble the distribution around a single horizontal cylinder in natural convection. The velocities in the inner-cylinder boundary layer can be made similar at any angle by using a length scale proportional to $Ra_L^{\frac{1}{4}}$ with the maximum velocity proportional to $Ra_L^{\frac{1}{2}}$. This cannot be extended very far into the gap since other effects predominate in the core. The velocity profiles in the outer-cylinder boundary layer in the top half of the annulus ($30° \leqslant \theta \leqslant 90°$) are independent of angular position with the magnitudes proportional to $Ra_L^{\frac{1}{4}}$. As the fluid moves down past the 90° position the outer boundary layer weakens, and disappears entirely near the bottom.

On the basis of previous experimental observations (Powe *et al.* 1969) and the lack of convergence of the present numerical results an oscillating laminar flow regime begins near a Rayleigh number of 10^5 for air. Fluids with a larger Prandtl number will remain steady until larger Rayleigh numbers are attained. This was observed by Liu *et al.* (1961) and confirmed by the present experimental results for water. Figure 12 shows streamlines and isotherms at $Ra_L = 10^5$ and $Pr = 5{\cdot}0$. The maximum of the stream function is about 15° from the top with the lower portion of the annulus practically stagnant. The vorticity is approaching zero in the central portion of the annulus, indicating the beginning of a stationary core region. This has also been found for natural convection in a vertical slot by Rubel & Landis (1969).

As the Rayleigh number is increased further the flow above the inner cylinder will become turbulent. This will create a turbulent boundary layer on the outer cylinder while the inner boundary layer remains laminar as reported by Lis (1966). Eventually the inner boundary layer will also become turbulent.

The local equivalent conductivities for the inner and outer cylinders are shown as a function of Rayleigh number in figures 13(*a*) and (*b*). The values approach one in the conduction regime for Rayleigh numbers below 10^2. The local

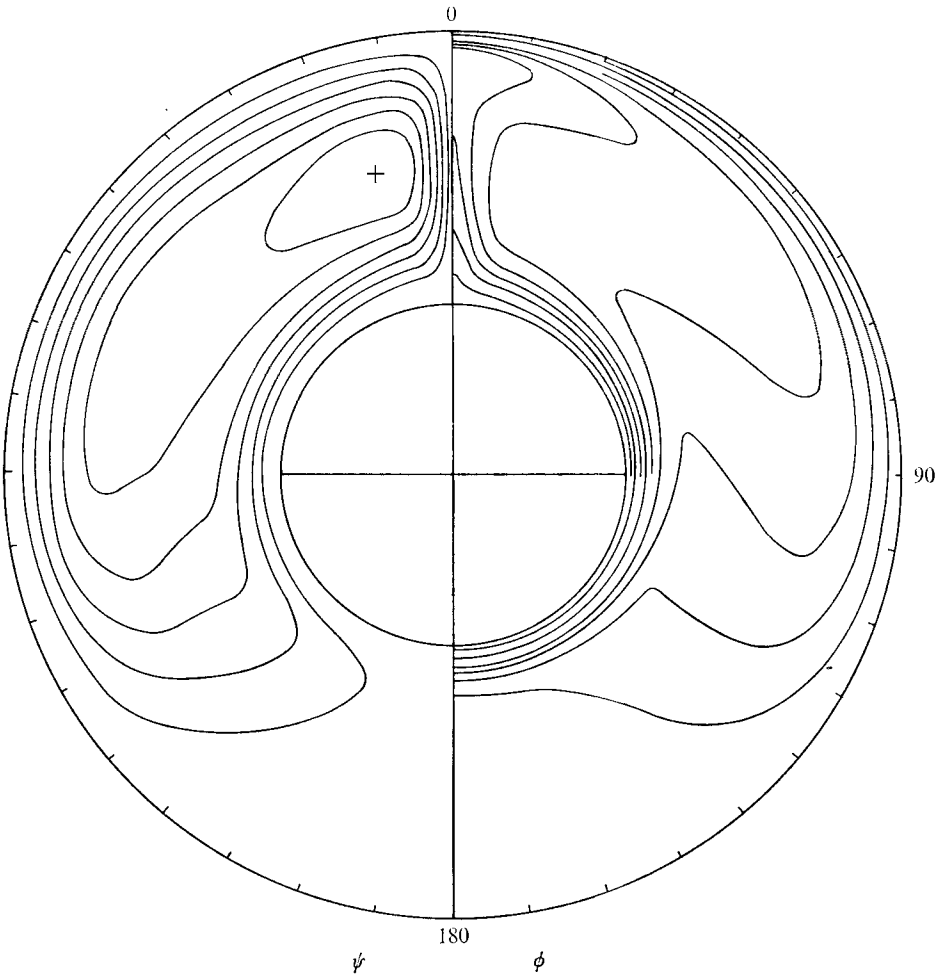

FIGURE 12. Streamlines and isotherms in steady laminar boundary-layer region for $Ra_L = 10^5$, $Pr = 5{\cdot}0$, $L/D_i = 0{\cdot}8$, $\Delta\psi = 5{\cdot}0$, $\Delta\phi = 0{\cdot}1$.

values for the inner cylinder are nearly proportional to $Ra_L^{\frac{1}{4}}$ in the steady laminar boundary-layer regime above $Ra_L = 3 \times 10^4$. However, this is not true for the outer cylinder. On both cylinders some local values are larger than one while others are less than one at the same Rayleigh number.

Simple reasoning predicts the highest local heat flux to occur at the stagnation point with small heat transfer at the separation point. Considering the inner cylinder, the local heat flux at the bottom is the largest while that at the top is small. The value of k_{eq} at the separation point is not zero but is less than one. The same argument applies to the outer cylinder with the stagnation point on top and separation near the bottom. The average equivalent conductivity is proportional to $Ra_L^{0{\cdot}245}$ above $Ra_L = 2 \times 10^4$.

The effect of diameter ratio on the results was determined by varying L/D_i from 0·1 to 8·0 near $Ra_L = 10^4$ and $Pr = 0{\cdot}7$. The flow pattern does not change

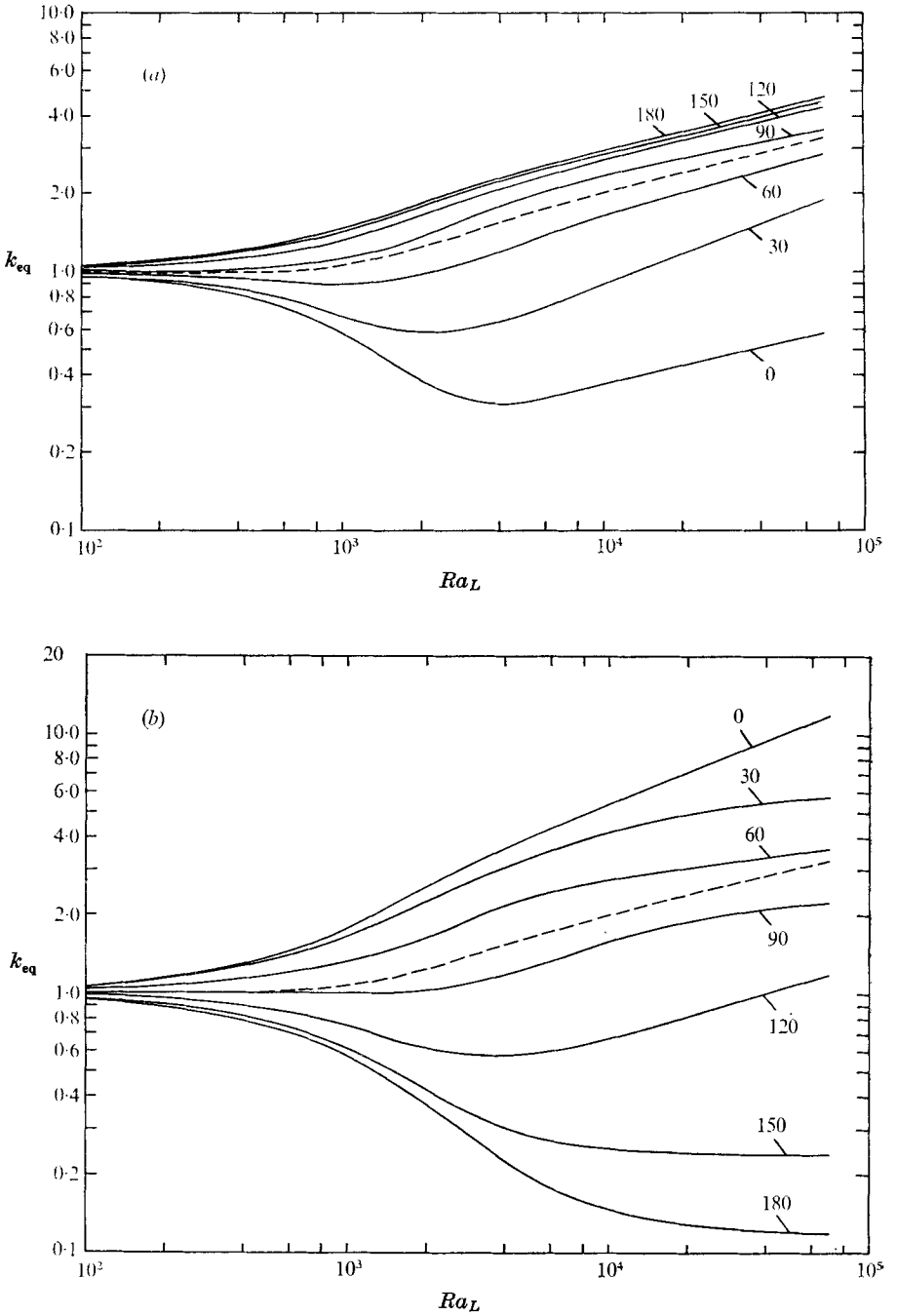

FIGURE 13. Influence of Rayleigh number on (*a*) inner- and (*b*) outer-cylinder local equivalent conductivity. – – – –, average.

significantly although the centre of rotation moves towards the top with increasing L/D_i. The mean equivalent conductivity is closely proportional to $[L/(R_i R_o)^{\frac{1}{2}}]^{\frac{1}{4}}$, where R_i and R_o are the inner and outer radii respectively, for $0{\cdot}1 \leqslant L/D_i \leqslant 1{\cdot}3$. This is similar to a correlation given by MacGregor & Emery (1968) for natural convection in vertical layers. The power of the Rayleigh number in the relation $\bar{k}_{eq} \approx CRa_L^n$ changes from near 0·25 for $L/D_i = 0{\cdot}5$ to 0·2 for $L/D_i = 8{\cdot}0$. The maximum mean equivalent conductivity occurs near $L/D_i = 3{\cdot}0$ at $Ra_L = 10^4$ but occurs at smaller values of L/D_i at larger Rayleigh numbers. However, the mean Nusselt number based on the inner-cylinder diameter increases as the outer cylinder is made larger at a constant Rayleigh number based on the inner-cylinder diameter. As the outer cylinder becomes larger relative to the inner cylinder the mean temperature in the annulus decreases. This indicates that the thermal resistance around the inner cylinder is becoming the dominant factor in the overall heat transfer. As the outer cylinder becomes infinitely large the only thermal resistance is around the inner cylinder with the temperature in the gap equal to that of the outer cylinder. At large L/D_i the total heat flow will be essentially that from a single horizontal cylinder in an infinite medium.

The Prandtl number was varied from 0·5 to 1000 at $Ra_L = 10^4$ and $L/D_i = 0{\cdot}8$. Local equivalent conductivities were generally smaller and more uniform at lower Prandtl numbers, indicating an approach to conduction. The centre of rotation moved nearer the top as the Prandtl number increased. For Prandtl numbers larger than 10, the flow and heat transfer remained virtually independent of Prandtl number. Local heat-transfer results for some of the numerical solutions are presented in table 2.

4. Comparison of experimental and numerical results

One of the objectives of the numerical study was to duplicate the conditions of the experiments. This not only serves as a check on the experiments but also provides information on the velocities which were not obtained experimentally. Since only the temperature distributions and heat transfer were measured experimentally the comparison is limited to these quantities.

The experimental temperature distributions from the interferograms can be directly compared with a polar plot of the temperature distribution obtained numerically under the same conditions. The right half of figure 14 (plate 4) is an interferogram of an air run. The fringes represent isotherms between the cylinders. The experimental errors are primarily optical and due to imperfect isothermal adjustment of the interferometer as well as end effects. The left half of figure 14 is a plot of the isotherms obtained from the corresponding numerical solution. The dimensionless temperature of these contours was chosen to be the same as those obtained experimentally on the right. The errors in the numerical result *arise from the constant-property assumption, the finite number of nodes, the* convergence level of the solution and the necessity to cross plot the results. The agreement, though not perfect owing to the considerations mentioned above, is quite good, lending validity to both methods.

				k_{eq}							
Ra_L	Pr	L/D_i	Location	0°	30°	60°	90°	120°	150°	180°	$\bar{k}_{eq}$
10^2	0.7	0·8	Inner	0·95	0·96	0·98	1·00	1·02	1·04	1·05	1·000
			Outer	1·06	1·05	1·03	1·00	0·97	0·95	0·94	1·002
10^3	0·7	0·8	Inner	0·57	0·67	0·90	1·14	1·32	1·44	1·47	1·081
			Outer	1·78	1·64	1·33	1·00	0·75	0·61	0·57	1·084
3×10^3	0·7	0·8	Inner	0·32	0·61	1·10	1·58	1·88	2·04	2·10	1·404
			Outer	3·19	2·72	1·91	1·11	0·59	0·35	0·28	1·402
6×10^3	0·7	0·8	Inner	0·33	0·74	1·38	2·00	2·34	2·50	2·56	1·736
			Outer	4·38	3·52	2·41	1·33	0·60	0·27	0·18	1·735
10^4	0·7	0·8	Inner	0·37	0·90	1·64	2·33	2·70	2·85	2·90	2·010
			Outer	5·35	4·10	2·72	1·54	0·68	0·26	0·14	2·005
2×10^4	0·7	0·8	Inner	0·44	1·18	2·01	2·73	3·21	3·34	3·41	2·405
			Outer	7·02	4·87	3·04	1·86	0·82	0·24	0·13	2·394
3×10^4	0·7	0·8	Inner	0·48	1·41	2·25	2·95	3·52	3·66	3·79	2·661
			Outer	8·42	5·25	3·21	2·05	0·92	0·24	0·13	2·643
5×10^4	0·7	0·8	Inner	0·53	1·68	2·58	3·28	3·97	4·15	4·32	3·024
			Outer	10·77	5·57	3·45	2·28	1·10	0·26	0·12	2·973
7×10^4	0·7	0·8	Inner	0·56	1·84	2·82	3·57	4·32	4·56	4·76	3·308
			Outer	12·91	5·77	3·65	2·43	1·19	0·21	0·12	3·226
10^4	5·0	0·8	Inner	0·43	1·20	1·72	2·23	2·64	2·89	2·98	2·069
			Outer	5·93	4·18	2·62	1·56	0·75	0·27	0·12	2·066
3×10^4	5·0	0·8	Inner	0·44	1·67	2·37	2·94	3·44	3·77	3·90	2·741
			Outer	7·80	5·37	3·66	2·38	1·03	0·27	0·10	2·768
5×10^4	5·0	0·8	Inner	0·70	1·91	2·52	3·17	3·75	4·15	4·36	3·036
			Outer	10·67	5·11	3·54	2·37	1·23	0·24	0·12	3·088
10^5	5·0	0·8	Inner	0·78	2·26	3·04	3·86	4·69	5·32	5·53	3·756
			Outer	16·86	5·52	3·99	2·78	1·21	0·20	0·09	3·471
10^4	0·5	0·8	Inner	0·34	0·77	1·53	2·33	2·69	2·79	2·84	1·950
			Outer	4·92	3·91	2·82	1·56	0·65	0·26	0·16	1·955
10^4	1·0	0·8	Inner	0·39	1·00	1·68	2·30	2·69	2·88	2·94	2·038
			Outer	5·74	4·16	2·66	1·54	0·70	0·26	0·14	2·039
10^4	10·0	0·8	Inner	0·43	1·22	1·73	2·22	2·63	2·88	2·97	2·070
			Outer	5·87	4·18	2·63	1·57	0·76	0·28	0·12	2·067
10^4	100·0	0·8	Inner	0·44	1·24	1·73	2·21	2·62	2·88	2·97	2·071
			Outer	5·84	4·19	2·64	1·57	0·76	0·28	0·12	2·067
10^4	0·7	0·1	Inner	0·14	0·45	0·81	1·37	1·75	2·01	2·10	1·271
			Outer	3·34	1·90	1·76	1·24	0·72	0·42	0·33	1·276
10^4	0·7	0·5	Inner	0·23	0·71	1·38	2·16	2·55	2·76	2·84	1·850
			Outer	4·87	3·57	2·59	1·50	0·68	0·28	0·16	1·853
10^4	0·7	1·0	Inner	0·46	0·98	1·72	2·37	2·74	2·87	2·91	2·061
			Outer	5·59	4·29	2·75	1·54	0·67	0·25	0·15	2·059
10^4	0·7	1·3	Inner	0·55	1·07	1·79	2·41	2·76	2·88	2·91	2·108
			Outer	5·82	4·46	2·79	1·53	0·65	0·24	0·15	2·110
10^4	0·7	2·0	Inner	0·71	1·16	1·84	2·42	2·77	2·89	2·92	2·148
			Outer	6·06	4·64	2·82	1·51	0·64	0·24	0·15	2·157
10^4	0·7	6·0	Inner	1·02	1·26	1·72	2·13	2·39	2·52	2·55	1·968
			Outer	5·97	4·61	2·70	1·36	0·57	0·23	0·15	2·084
10^4	0·7	8·0	Inner	1·05	1·23	1·63	2·00	2·26	2·40	2·44	1·878
			Outer	5·89	4·54	2·65	1·33	0·55	0·23	0·15	2·051

TABLE 2. Local heat-transfer results from numerical solutions

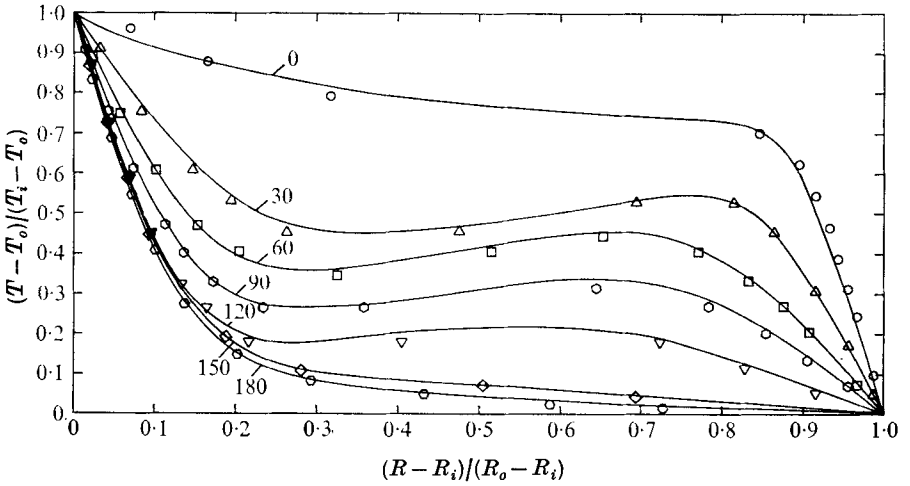

FIGURE 15. Comparison of experimental and numerical dimensionless radial temperature profiles. Experimental data points: ○, 0°, △, 30°; □, 60°; ◇, 90°; ▽, 120°; ◇, 150°; ○, 180°.

	Experimental	Numerical
Ra_L	$4{\cdot}7 \times 10^4$	5×10^4
Pr	0·706	0·7
L/D_i	0·8	0·8

Another method of comparison is to evaluate the radial dimensionless temperature profiles. This is done in figure 15 for the results shown in figure 14. Additional experimental errors arise owing to the necessity of estimating the centre of fringes and the need to extrapolate temperature curves to the cylinder walls. The agreement is still good, particularly in the boundary layers adjacent to each cylinder. The fringes are narrower in these regions, which enables their locations to be determined more accurately than in the centre of the annulus.

A comparison of the local equivalent conductivities for the above results is given in figure 16. Again the agreement is good. The largest difference between the experimental and numerical values is less than 10 % while the average values are within 2 % of each other.

Comparisons of some of the water results with corresponding numerical solutions have also been made with equal successs. The water results should agree better than those for air since the initial optical adjustment was better and the small temperature differences used for water come closer to approximating the constant-property assumption used in the numerical calculations. The maximum temperature difference for air was 69 °C compared with 2·4 °C for water.

Figure 7 shows the measured average equivalent conductivities for the air and water tests as well as the numerical results for $Pr = 0{\cdot}7$ and $L/D_i = 0{\cdot}8$. The maximum deviation of the air results from the calculated values is 3 % with the average deviation less than 2 %. The water results are slightly higher than those for air owing to the larger Prandtl number of water.

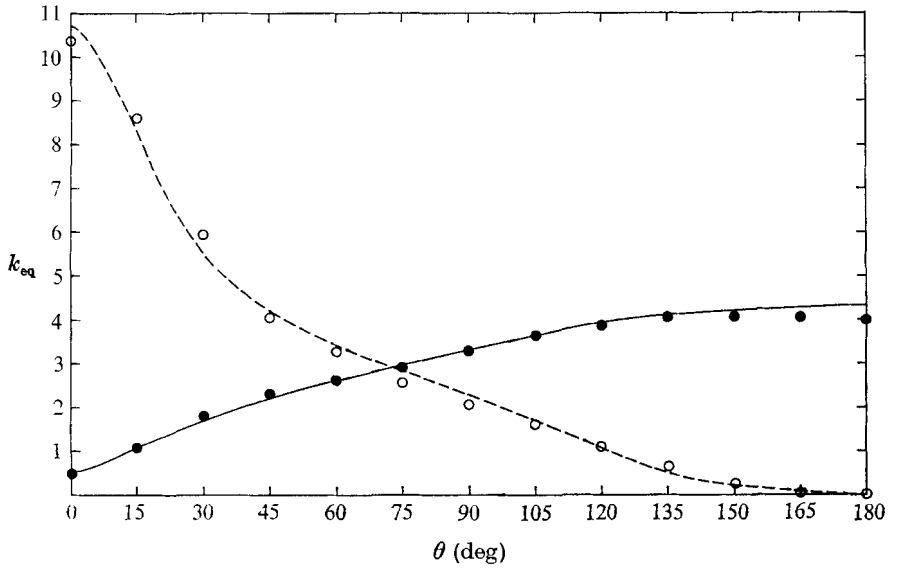

FIGURE 16. Comparison of experimental and numerical local equivalent conductivity.

	Experimental	Numerical
Ra_L	$4{\cdot}7 \times 10^4$	5×10^4
Pr	0·706	0·7
L/D_i	0·8	0·8
Inner cylinder	●	——
Outer cylinder	○	– – –

On the basis of the good agreement between the experimental and numerical results, it seems possible to determine heat-transfer parameters for free convection in enclosures using either method. The experiments have the advantage of being applicable to unsteady flow and turbulence, where the numerical computations become unstable. However the numerical analysis gives more information, including the velocity field, which is difficult to obtain experimentally.

5. Summary

The results of an experimental and numerical study of natural convection flow between horizontal isothermal concentric cylinders have been presented. Quantities obtained experimentally include temperature distributions and local and averaged heat-transfer coefficients. The numerical solutions confirm these values, provide the corresponding velocity distribution and extend the results to lower Rayleigh numbers.

Interferograms were obtained using both air and water for $L/D_i = 0{\cdot}8$. The temperature distributions for both fluids were nearly the same at similar Rayleigh numbers. Some aspects of the temperature distributions have been found to occur for natural convection in other geometries, including a single horizontal cylinder, concentric spheres and vertical fluid layers. The flow was steady for all Rayleigh

numbers investigated. Local equivalent conductivities were obtained for both the inner and the outer cylinder. Mean heat-transfer results obtained by measuring the power input agreed with the averaged optical measurements.

Numerical solutions covered the range of Rayleigh numbers from pure conduction to steady laminar boundary-layer flow for $L/D_i = 0{\cdot}8$. The influence of diameter ratio and Prandtl number was determined near a Rayleigh number of 10^4. Temperature distributions and local equivalent conductivities agreed with the corresponding experimental data.

Radial temperature length scales in the inner-cylinder boundary layer and the inner-cylinder local heat flux were found to be closely proportional to $Ra_L^{-\frac{1}{4}}$ for $Pr = 0{\cdot}7$, $L/D_i = 0{\cdot}8$ and $3 \times 10^4 \leqslant Ra_L \leqslant 10^5$. The maximum stream function in the annulus and the angular velocities were proportional to $Ra_L^{\frac{1}{4}}$ for the same range of parameters.

The authors gratefully acknowledge the support received from the National Science Foundation through Grants GK 15252 and 75-01091, computer time granted by the University of Minnesota Computer Center and for one author (T.H.K.) the receipt of a National Defense Education Act IV Fellowship.

REFERENCES

ABBOTT, M. R. 1964 A numerical method for solving the equations of natural convection in a narrow concentric cylindrical annulus with a horizontal axis. *Quart. J. Mech. Appl. Math.* **17**, 471–481.

BARELKO, V. V. & SHTESSEL, E. A. 1973 On a heat-transfer law for free convection in cylindrical and spherical layers. *Int. Chem. Engrs*, **13**, 479–483.

BATCHELOR, G. K. 1954 Heat transfer by free convection across a closed cavity between vertical boundaries at different temperatures. *Quart. Appl. Math.* **12**, 209–233.

BECKMANN, W. 1931 Die Wärmeübertragung in zylindrischen Gasschichten bei natürlicher Konvektion. *Forsch. Geb. d. Ingenieurwesen*, **2** (5), 165–178.

BERKENGEIM, A. A. 1966 An investigation of natural convection in cylindrical liquid layers. *Inzh.-Fiz. Zh.* **10**, 459–464.

BISHOP, E. H. 1966 *Discussion 3rd Int. Heat Transfer Conf. Chicago*, **2** (session 6), 155–156.

BISHOP, E. H. & CARLEY, C. T. 1966 Photographic studies of natural convection between concentric cylinders. *Proc. 1966 Heat Transfer Fluid Mech. Inst.* pp. 63–78.

BISHOP, E. H., CARLEY, C. T. & POWE, R. E. 1968 Natural convective oscillatory flow in cylindrical annuli. *Int. J. Heat Mass Transfer*, **11**, 1741–1752.

CRAWFORD, L. & LEMLICH, R. 1962 Natural convection in horizontal concentric cylindrical annuli. *I. E. C. Fund.* **1**, 260–264.

ECKERT, E. R. G. 1960 *The Collected Works of Irving Langmuir*, introduction to part 1, vol. 2. Pergamon.

ECKERT, E. R. G. & SOEHNGEN, E. E. 1948 Studies on heat transfer in laminar free convection with the Zehnder–Mach interferometer. *Wright-Patterson AFB Tech. Rep.* no. 5747, ATI-44580.

GOLDSTEIN, R. J. 1970 Optical measurement of temperature. *Measurement Techniques in Heat Transfer, AGARDograph*, no. 130, pp. 177–228.

GOSMAN, A. D., PUN, W. N., RUNCHAL, A. K., SPALDING, D. B. & WOLFSHTEIN, M. 1969 *Heat and Mass Transfer in Recirculating Flows*. Academic.

GRIGULL, U. & HAUF, W. 1966 Natural convection in horizontal cylindrical annuli. *3rd Int. Heat Transfer Conf., Chicago*, pp. 182–195.

HAUF, W. & GRIGULL, U. 1970 Optical methods in heat transfer. *Adv. in Heat Transfer*, **6**, 133–366.

HODNETT, P. F. 1973 Natural convection between horizontal heated concentric circular cylinders. *J. Appl. Math. Phys.* **24**, 507–516.

HUETZ, J. & PETIT, J. P. 1974 Natural and mixed convection in concentric annular spaces – experimental and theoretical results for liquid metals. *5th Int. Heat Transfer Conf., Tokyo*, vol. 3, pp. 169–172.

ITOH, M., FUJITA, T., NISHIWAKI, N. & HIRATA, M. 1970 A new method of correlating heat-transfer coefficients for natural convection in horizontal cylindrical annuli. *Int. J. Heat Mass Transfer*, **13**, 1364–1368.

KOSHMAROV, Y. A. & IVANOV, A. Y. 1973 Experimental study of heat transfer through a rarefied gas between coaxial cylinders. *Heat Transfer, Sov. Res.* **5**, 29–36.

KRAUSSOLD, H. 1934 Wärmeabgabe von zylindrischen Flüssigkeitsschichten bei natürlicher Konvektion. *Forsch. Geb. d. Ingenieurwesen*, **5** (4), 186–191.

LIS, J. 1966 Experimental investigation of natural convection heat transfer in simple and and obstructed horizontal annuli. *3rd Int. Heat Transfer Conf., Chicago*, pp. 196–204.

LIU, C. Y., MUELLER, W. K. & LANDIS, F. 1961 Natural convection heat transfer in long horizontal cylindrical annuli. *Int. Developments in Heat Transfer, A.S.M.E.* pp. 976–984.

MACGREGOR, R. K. & EMERY, A. F. 1968 Free convection through vertical plane layers – moderate and high Prandtl number fluids. *A.S.M.E. Paper*, no. 68-HT-4.

MACK, L. R. & BISHOP, E. H. 1968 Natural convection between horizontal concentric cylinders for low Rayleigh numbers. *Quart. J. Mech. Appl. Math.* **21**, 223–241.

PEDERSEN, B. O., DOEPKEN, H. C. & BOLIN, P. C. 1971 Development of a compressed-gas-insulated transmission line. *I.E.E.E. Winter Power Meeting*, paper 71 TP 193-PWR.

POWE, R. E. 1974 Bounding effects of the heat loss by free convection from spheres and cylinders. *J. Heat Transfer, A.S.M.E.* **96**, 558–560.

POWE, R. E., CARLEY, C. T. & BISHOP, E. H. 1969 Free convective flow patterns in cylindrical annuli. *J. Heat Transfer*, **91**, 310–314.

POWE, R. E., CARLEY, C. T. & CARRUTH, S. L. 1971 A numerical solution for natura convection in cylindrical annuli. *J. Heat Transfer*, **92** (12), 210–220.

RAITHBY, G. D. & HOLLANDS, K. G. T. 1975 A general method of obtaining approximate solutions to laminar and turbulent free convection problems. *Adv. in Heat Transfer*, **11**, 265–315.

ROTEM, Z. 1972 Conjugate free convection from horizontal conducting circular cylinders. *Int. J. Heat Mass Transfer*, **15**, 1679–1693.

RUBEL, A. & LANDIS, F. 1969 Numerical study of natural convection in a vertical rectangular enclosure. *Phys. Fluids Suppl.* **12**, II 208–213.

SCANLAN, J. A., BISHOP, E. H. & POWE, R. E. 1970 Natural convection heat transfer between concentric spheres. *Int. J. Heat Mass Transfer*, **13**, 1857–1872.

SHIBAYAMA, S. & MASHIMO, Y. 1968 Natural convection heat transfer in horizontal concentric cylindrical annuli. *Papers J.S.M.E. Nat. Symp.* no. 196, pp. 7–20.

VOIGT, H. & KRISCHER, O. 1932 Die Wärmeübertragung in zylindrischen Luftschichten bei natürlicher Konvektion. *Forsch. Geb. d. Ingenieurwesen*, **3** (6), 303–306.

ZAGROMOV, Y. A. & LYALIKOV, A. S. 1966 Free convection heat transfer in horizontal cylindrical layers with different positions of the heated element. *Inzh.-Fiz. Zh.* **10** (5), 577–583.

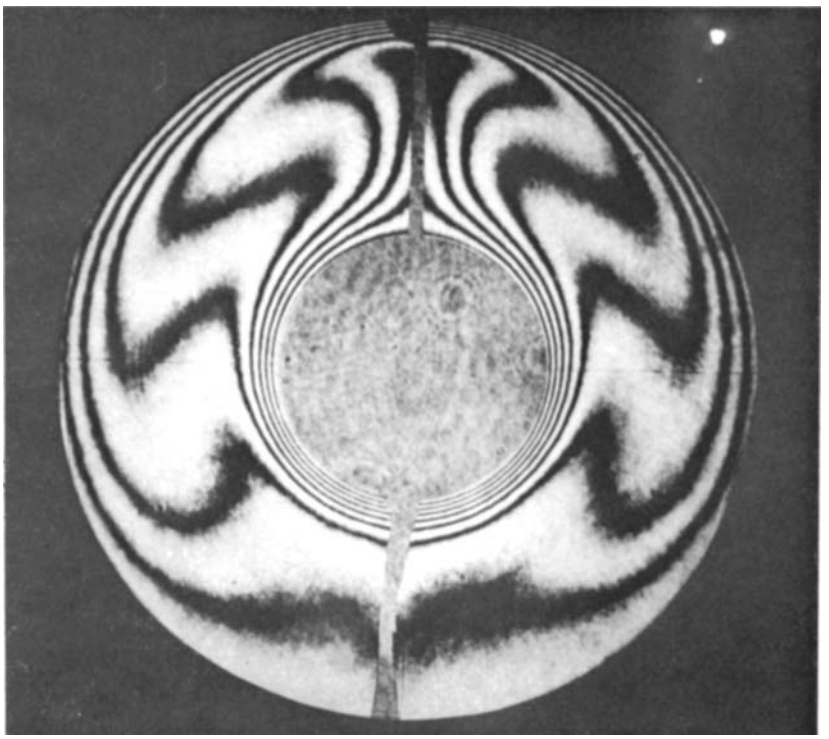

FIGURE 2. Interferogram taken using air for $Ra_L = 4{\cdot}70 \times 10^4$, $Pr = 0{\cdot}706$, $L/D_i = 0{\cdot}8$.

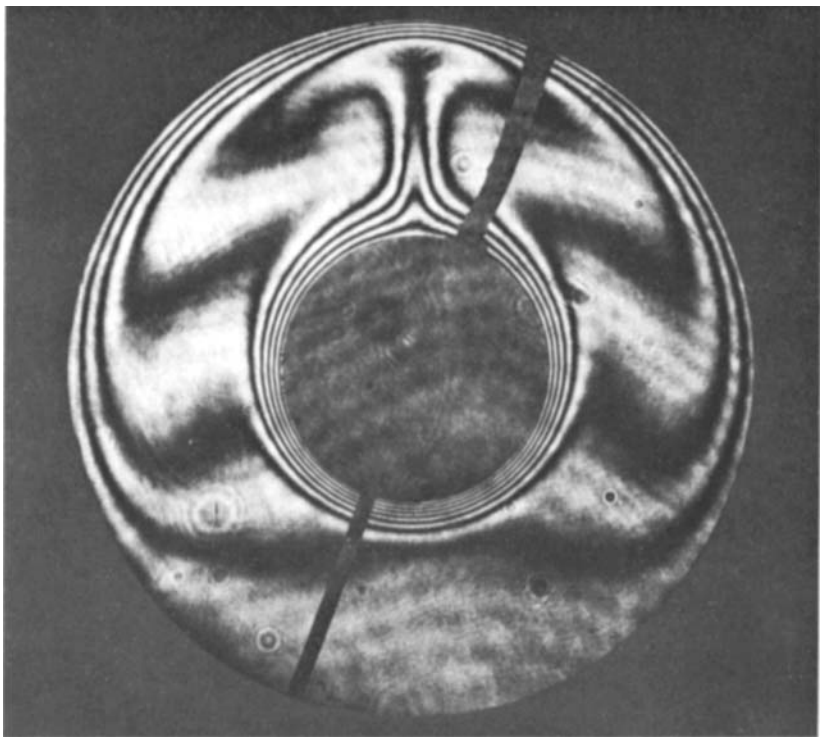

FIGURE 3. Interferogram taken using water for $Ra_L = 9{\cdot}52 \times 10^4$, $Pr = 6{\cdot}21$, $L/D_i = 0{\cdot}8$.

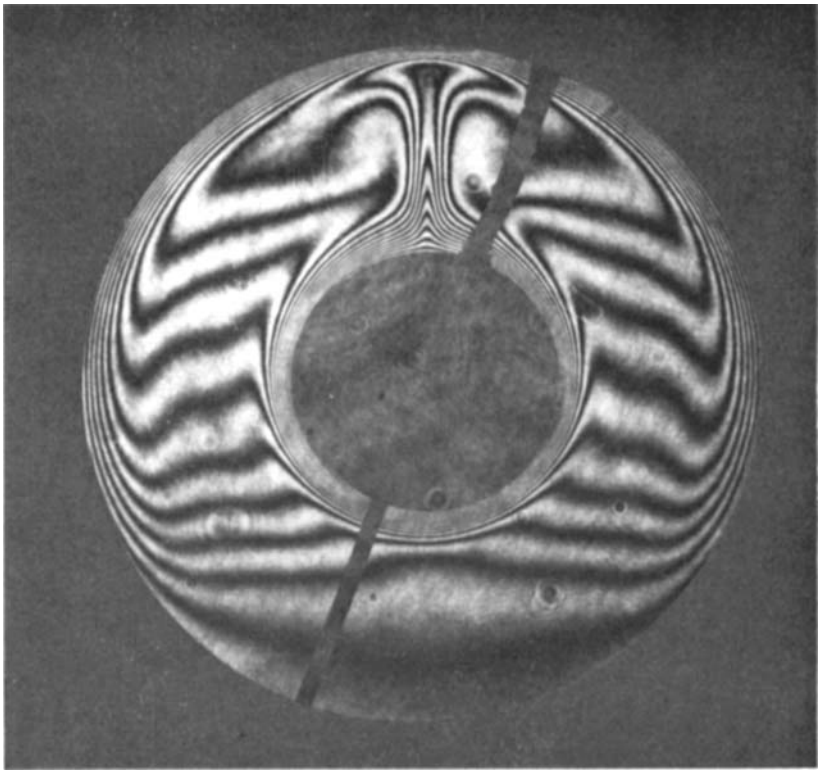

FIGURE 4. Interferogram taken using water for $Ra_L = 2{\cdot}33 \times 10^5$, $Pr = 6{\cdot}19$, $L/D_i = 0{\cdot}8$.

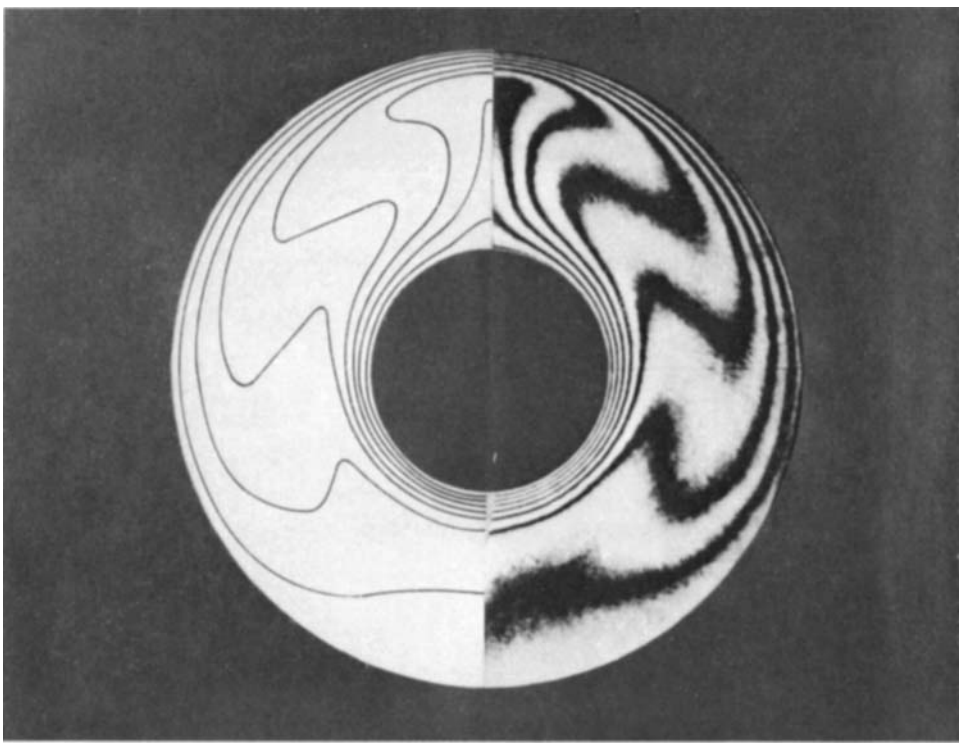

FIGURE 14. Comparison of experimental and numerical isotherms.

	Experimental	Numerical
Ra_L	$4{\cdot}7 \times 10^4$	5×10^4
Pr	0·706	0·7
L/D_i	0·8	0·8